Aspects 482: 424–427, 2015

which should be cited to refer to this work.

Interplay between internal structure and optical properties of thermosensitive nanogels

Mónica Ledesma-Motolinía[a], Marco Braibanti[b], Luis F. Rojas-Ochoa[c], Catalina Haro-Pérez[d,*]

[a] *Programa de Doctorado en Ciencias e Ingeniería de Materiales, Universidad Autónoma Metropolitana-Azcapotzalco, Av. San Pablo 180, 02200 México D.F., Mexico*
[b] *Department of Physics, University of Fribourg, CH-1700 Fribourg, Switzerland*
[c] *Departamento de Física, CINVESTAV-IPN, Av. Instituto Politécnico Nacional 2508, 07360 México D.F, Mexico*
[d] *Departamento de Ciencias Básicas, Universidad Autónoma Metropolitana-Azcapotzalco, Av. San Pablo 180, 02200 México D.F., Mexico*

HIGHLIGHTS

- We study the internal structure of PNIPAM microgels as a function of temperature.
- Core and external radius of PNIPAM particles is determined by light scattering.
- The microgel refractive index, measured by refractometry, increases with temperature.
- We propose a radial profile for the particle refractive index to describe the experiments.
- From the analysis, we determine the refractive index of the microgel core.

GRAPHICAL ABSTRACT

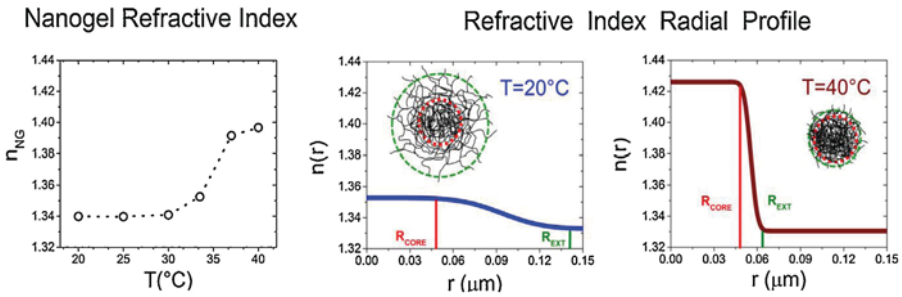

ABSTRACT

The structural and optical properties of thermosensitive particles, nanogels, are studied by light scattering and refractometry as a function of temperature. Nanogels are composed of poly- *N*-Isopropopylacrylamide, a polymer that shrinks at temperatures higher than its lower critical solution temperature, 33 °C. The internal nanogel structure obtained by light scattering is well modeled by assuming a constant radial mass density profile convoluted with a Gaussian function. Moreover, we introduce a simple method that allows us to describe the measured temperature-dependent index of refraction of these complex nanoparticles by using their structural information, core dimension and external radius.

1. Introduction

In the last decades, nanogels have been subject of numerous studies due to their numerous technological applications [1–4] and their use as model systems to investigate fundamental phenomena in soft materials [5–8]. One of the interesting properties of these particles is their capacity of reducing their size as the temperature increases due to a change in the interactions between water and polymer chains. Above a certain temperature, the lower critical solution temperature (LCST), Poly-NIPAM becomes hydrophobic causing the collapse of the particle and the subsequent expulsion of water from the nanogel interior [9]. At this transition, that occurs at around 33 °C for this polymer, not only the particle size changes abruptly, but also does the polymer mass density distribution inside

* Corresponding author.
E-mail address: cehp@correo.azc.uam.mx (C. Haro-Pérez).

the particle, which induces a sudden variation of its optical properties. For example, the refractive index of nanogel particles strongly depends on temperature and exhibits an abrupt increase around the LCST [10]. The temperature dependence of the internal structure of Poly-NIPAM particles has been analyzed by measuring the particle form factor by means of neutron [11–13] and light scattering [14]. In all cases, the authors find that a non-constant mass density profile accounts for the heterogeneous structure of the PNIPAM particles due to an uneven distribution of crosslinker inside the particle. This profile describes an inner denser region, named core, and a shell with a non-constant mass density that decreases gradually from the edge of the core toward the particle surface.

In this paper we assume a mass density profile defined by a convolution of a box with a Gaussian function to describe the particle form factor measured by light scattering [11]. From the analysis of the scattering vector behavior of the scattered light as a function of temperature, we obtain the temperature dependence of the structural parameters, core and overall particle dimensions. The structural information is used to describe the effective refractive index of PNIPAM particles by assuming a radial dependence for the particle refractive index similar to that of the mass density profile. The validity of this model has been confirmed on two different nanogels systems with different degree of crosslinking. The approach used in this study could be useful for the engineering of nanogel systems with potential applications in optics as tunable photonic materials [15,16] and optical tagging [17], among others.

2. Experimental system

In this work PNiPAM particles are synthesized in emulsion-polymerization as described in Ref. [6]. The monomer *N*-isopropylacrylamide, NiPAM (7.9 g), the crosslinker *N,N*-methylenbisacrylamide, BIS (0.15 g), and the stabilizer sodium dodecylsulfate, SDS (0.15 g), are dissolved in 450 ml of pure water. In parallel, a solution of the initiator potassium peroxodisulfate, KPS (0.6 g), in 50 ml of pure water is prepared in a separate flask. After bubbling both solutions with nitrogen for 30 min, the initiator is injected in the mixture that contains the monomer, which has been previously heated to 70 °C. The polymerization process is terminated after 5 h and, finally, the dispersion is cooled down to room temperature and purified by dialysis and several centrifugation steps. The solid content of our final stock solution is ~3.1%w/w, and the particle number density is ~ 54 particles/μm^3. We should mention that our system at quasideionized conditions exhibits a liquid-crystal transition as a function of concentration at 25 °C. This feature indicates a low size polydispersity of our nanogels and allows us to unambiguously determine the particle number density of the crystalline samples from the Bragg peak positions [18], measured by static light scattering with a 3D-DLS scattering device (LS Instruments AG, Fribourg, Switzerland). The device is provided with a multitau digital correlator (Flex) and uses a He–Ne laser as a light source, wavelength $\lambda = 632.8$ nm. As a result, from both the dry solid content and the particle number concentration we obtain the polymer mass per particle being ~5.78 10^{-16} g.

3. Results and discussion

The structural characterization of the resulting nanoparticles is made by measuring the particle form factor, $P(q)$, by static light scattering (SLS) as a function of temperature. The q -dependence of the scattered light, shown as symbols in Fig. 1(a), becomes less pronounced as the temperature increases as a consequence of the collapse of the poly-NIPAM particles. In order to obtain information about particle dimensions we use a model that assumes

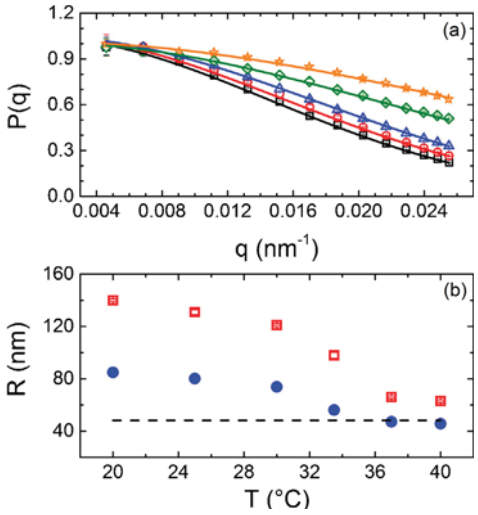

Fig. 1. (a) Particle form factor measured by static light scattering at 20 °C (black squares), 25 °C (red circles), 30 °C (blue triangles), 33.5 °C (green diamonds) and 37 °C (orange stars). Lines are fits to the data by assuming a non-constant mass density profile [11]. (b) Temperature dependence of the external (hydrodynamic) radius (open squares), the Guinier radius (solid circles) and the core radius (dashed line) (For interpretation of the references to colour in this figure legend, the reader is referred to the web version of this article.).

a non-constant radial particle density, which is valid under the Rayleigh-Gans-Debye approximation (RGD) [11]. In this model the radial density decreases from the edge of the core toward the surface of the particle and is calculated as a convolution of a radial box of dimension R and a Gaussian function. In this way, the form factor is given by $P(q) = \left[\frac{3[\sin(qR)-qR\cos(qR)]}{(qR)^3}\exp(-\frac{(\sigma q)^2}{2})\right]^2$, where σ accounts for the width of the smeared particle surface and it is defined as $\sigma = 0.25\,(R_{Ext} - R_C)$, R_{Ext} is the overall radius of the particle and R_C is the core radius. R represents the distance from the particle center to the point where the density has decreased to half of the core density and it can be expressed as $R = 0.5\,(R_{Ext} + R_C)$ [11]. The fit to the experimental data, shown as lines in Fig. 1(a), indicates that this model describes well our experiments. Since we have observed crystallization of the deionized suspensions, which is only possible for enough monodisperse dispersions, in the analysis we have omitted size polydispersity effects. We perform a global fit to the form factors measured at all temperatures considering that the core radius does not depend on temperature, as reported previously [12], and using the hydrodynamic radius, R_H, measured by dynamic light scattering as an estimate of the external radius, $R_{Ext} = R_H$. The core radius obtained from this fitting procedure is $R_C = (48.1 \pm 0.5)$ nm. The temperature dependent values of the external radius are shown as open squares in Fig. 1(b), where we can observe that R_{Ext} slightly decreases until the temperature reaches the LCST. Around the transition temperature, the external radius decreases abruptly due to the sudden shrink of the particle and remains almost constant for higher temperatures. We find that our results are similar to those reported for a similar system [11]. Additionally, the radius of gyration R_g obtained from the Guinier analysis of ln $[I(q)]$ vs q^2 depicts a similar behavior with temperature, as shown in Fig. 1(b) as solid circles. We should note that in the collapsed state of the particle, at 40 °C, the ratio between the radius of gyration and the external radius is $R_g(40\,°C)/R_{Ext}(40\,°C) = 46\,nm/63\,nm = 0.73$, a value compatible with the ratio R_g/R_{Ext} for a compact sphere $R_g/R_{Ext} = (3/5)^{0.5} = 0.774$. By contrast, in the globular state, at 20 °C, the ratio $R_g(20\,°C)/R_{Ext}(20\,°C) = 85\,nm/141\,nm = 0.61$, value that is below the ratio expected for compact spheres indicating a less dense structure of the nanogel in the globular state. These results suggest a non-constant radial profile of the mass inside the particle

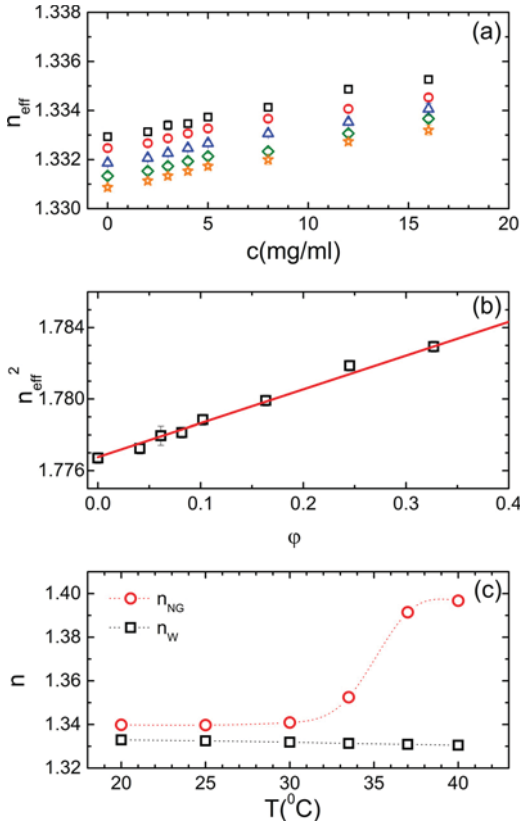

Fig. 2. (a) Concentration dependence of the effective refractive index of nanogel suspensions, n_{eff}, measured at different temperatures: 20 °C (black squares), 25 °C (red circles), 30 °C (blue triangles), 33.5 °C (green diamonds) and 37 °C (orange stars). (b) $n_{\text{eff}}{}^2$ versus particle volume fraction at 20 °C. The red line is the best fit to $n_{eff}^2 = \left(n_{NG}^2 - n_w^2\right)\varphi + n_w^2$ (c) Nanogel refractive index, n_{NG}, (open circles) and water refractive index, n_w, (open squares) obtained from experiments as a function of temperature (For interpretation of the references to color in this figure legend, the reader is referred to the web version of this article.).

and justify the use of the Stieger's model to describe our measurements.

After describing the internal structure of our nanogel particles we characterize their optical properties by measuring their refractive index. The temperature dependence of the nanogel refractive index n_{NG} was obtained by measuring the concentration dependence of the effective refraction index of nanogel dispersions, n_{eff}, at different temperatures using an Abbe NAR-1T Liquid refractometer working at a wavelength of 589 nm. The selected temperature range goes from 20 °C to 40 °C, which includes the LCST, in order to study the optical properties in the transition regime from the globular to the collapsed state of the nanoparticles. The experimental values of the effective refractive index increase with concentration as shown in Fig. 2(a). Assuming the Newton mixing rule for the index of refraction of a colloidal suspension, the effective refractive index of the nanogel suspension can be expressed as $n_{eff}^2 = (n_{NG}^2 - n_w^2)\varphi + n_w^2$ [19–21], with n_w being the refractive index of water, the refractive index of the nanogel particle n_{NG} can be obtained from linear fits to the data plotted as $n^2{}_{\text{eff}}$ versus φ, as shown in Fig. 2(b). In this case, the concentration of the sample is expressed in terms of particle volume fraction. For a given temperature, the volume fraction of the sample $\varphi(T)$ was obtained by multiplying the particle number density ρ by the volume occupied by a particle at that temperature $\varphi(T) = \rho\frac{4}{3}\pi R_{Ext}^3(T)$. The so obtained nanogel refractive indexes are plotted in Fig. 2(c) as a function of temperature. The nanogel refractive index exhibits a noticeable temperature dependence with a strong variation around the transition temperature. The refractive index goes from 1.34 at low temperatures to 1.40 at temperatures higher than the LCST. We also measured the temperature dependence of the water refractive index, reported as open squares in Fig. 2(c), and find a good agreement with previous results [22]. The obtained values of the particles effective refractive indexes together with the particles radii allow us to verify the RGD conditions for all temperatures, $|\frac{n_{NG}}{n_W} - 1| \ll 1$ and $\frac{2\pi n_W R}{\lambda}|\frac{n_{NG}}{n_W} - 1| \ll 1$. In the extreme case, at 40 °C, values of 0.07 and 0.043 are obtained for the two conditions, respectively.

In order to describe the optical properties of the nanogels we use the structural information obtained from SLS to compute the nanogel refractive index, n_{NG}, by using [23]

$$n_{NG} = V^{-1}\int_0^{R_{Ext}} n(r)\,4\pi r^2 dr \qquad (1)$$

where V is the volume of a single nanogel particle and R_{ext} is the external radius of the particle. The refractive index $n(r)$ is assumed to have the same radial dependence as the mass density profile found in static light scattering experiments [11]: a convolution of a radial box of dimension R, $u(r) = \left\{\begin{array}{ll} 1 & r \le R \\ 0 & r > R \end{array}\right\}$, with a Gaussian function, $g(r) = \frac{1}{\sqrt{2\pi}\sigma}\exp\left(-\frac{r^2}{2\sigma^2}\right)$, where σ is the standard deviation of the Gaussian function and $R = R_C + 2\sigma$. In this way, the radial dependence of the refractive index is described by $n(r) = (n_C - n_W)[u(r) * g(r)] + n_W$, where n_C is the refractive index of the particle core and $u(r) * g(r)$ represents the convolution of the radial box and Gaussian functions. Note that $n(r=0) = n_C$ and $n(r = R_{\text{Ext}}) = n_{\text{W}}$. This radial dependence accounts for a higher contrast of the inner part of the particle and for its gradual decrease from the core edge toward the surface as an error function [11].

The core and particle dimensions used in the calculations are those obtained from the structural characterization shown in Fig. 1(b). The resulting refractive index profiles needed to describe the experiments are plotted in Fig. 3(a) at three different temperatures 20 °C (continuous line), 30 °C (dashed line) and 40 °C (dotted line). For the lower temperatures the refractive index profile exhibits an initial part where the refractive index is almost constant followed by a gradual decay toward the particles surface. This decay becomes abrupt when the temperature is higher than the LCST. An important result obtained from our description is that, along with the core mass density, also the nanogel core refractive index increases with temperature and exhibits a sudden change around the transition temperature. The increase of the particle core contrast with temperature can be explained as an effect of the increase of the mass density in the inner part of the nanogels as a function of temperature [11]. We should mention that we also performed the calculations by assuming a linear dependence of the radial refractive index from the core to the surface [12] and found negligible differences with the estimates of the core refractive index obtained from the Stieger's model.

Furthermore, we have applied our scheme to a different batch of nanogel particles having a higher crosslinker density. The new synthesis is obtained by following the protocol described in Section II, where we add 7.87 g of NIPAM, 0.6 g of BIS, 0.6 g of KPS and 0.05 g of SDS. In this case, we obtain a stock solution with a solid content of ~3.0%w/w, which roughly corresponds to a particle number density of 20 particles/μm^3 and a polymer mass per particle of 15.0 10^{-16} g. The resulting particles have a hydrodynamic radius of ~156 nm at 20 °C and ~83 nm at 40 °C. We find that they display a temperature dependence of their structural and optical properties similar to that of the first synthesis. Nevertheless, in this case we obtain from our analysis a higher core refractive index at all inves-

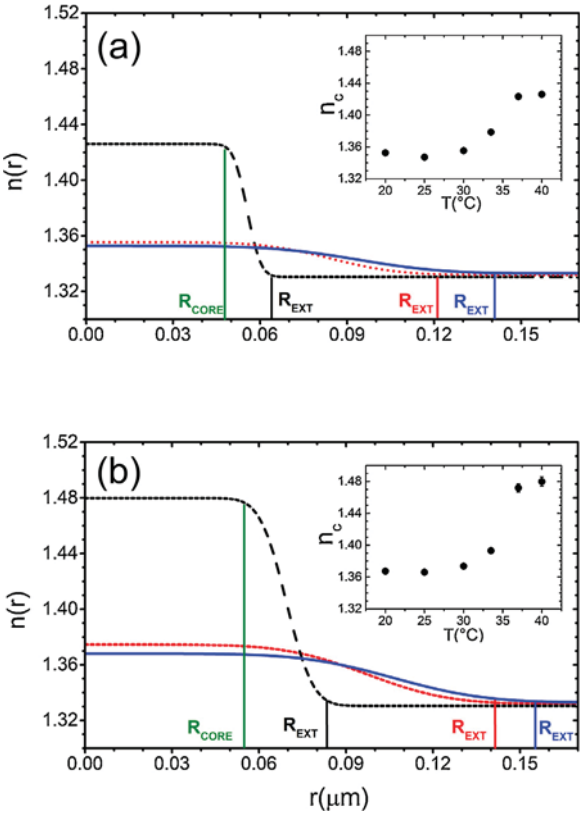

Fig. 3. Nanogel radial refractive index profile used in the theory to obtain the experimental nanogel refractive index values at 20 °C (solid line), 30 °C (dashed line) and 40 °C (dotted line). The vertical lines represent the core radius and the external radius at each temperature. Inset: Temperature dependence of the particle core refractive index used in the calculations. Nanogel particles having a BIS/NIPAM weight ratio of (a) 1.9% and (b) 7.6%.

tigated temperatures, shown in Fig. 3(b), which is consistent with the higher polymer mass density in the core of the new particles.

4. Conclusions

Here we present data on the behavior of the internal structure and effective refractive index of nanogel particles as a function of temperature. We show that the interesting optical properties of these particles can be described by assuming a constant radial density profile convoluted with a Gaussian function. Moreover, this model describes reasonably well the experimental particle form factor measured by light scattering allowing us to determine the internal structure of the nanogel, core dimension and external radius, information needed as an input to calculate the effective refractive index of the PNIPAM particles. As a result of the analysis, we can describe the radial profile of the refractive index. In particular, the refractive index of the densest region of the particle, the core, increases with temperature, which is in agreement with the temperature dependence of the core mass density as found in the literature for similar systems. In this work we describe a simple method to infer optical properties of nanogel particles from their structural data that, to our knowledge, has not been previously reported. We believe that our results represent a step toward the understanding of the subtle interplay between internal structure and optical properties of complex nanoparticles that could be of interest for basic and applied research, such as index matching of soft particles in materials science and designing of nanoparticles with tunable photonic properties.

Acknowledgments

C.H.P. and L.F.R.O. acknowledge financial support from Conacyt-Mexico, Grants Nos. 166645 and 154733, respectively.

References

[1] M. Das, H. Zhang, E. Kumacheva, Annu. Rev. Mater. Res. 36 (2006) 117.
[2] Smart Polymers: Applications in Biotechnology and Biomedicine, in: I. Galaev, B. Mattiasson (Eds.), 2nd ed., Taylor and Francis Group, Boca Raton, 2008), 2008.
[3] V.C. Lopez, J. Hadgraft, M.J. Snowden, Int. J. Pharm. 292 (2005) 137.
[4] J. Rubio Retama, B. Lopez-Ruiz, E. Lopez-Cabarcos, Biomaterials 24 (2003) 2965.
[5] B.R. Saunders, B. Vincent, Adv. Colloid Interface Sci. 80 (1999) 1.
[6] H. Senff, W. Richtering, J. Chem. Phys. 111 (1999) 1705.
[7] A. Moncho-Jordá, J.A. Anta, J. Callejas-Fernández, J. Chem. Phys. 138 (2013) 134902.
[8] S. Ahualli, A. Martín-Molina, M. Quesada-Pérez, Phys. Chem. Chem. Phys. 16 (2014) 25483.
[9] R. Pelton, Adv. Colloid Interface Sci. 85 (2000) 1.
[10] B.W. Garner, T. Cai, S. Ghosh, Z. Hu, A. Neogi, App. Phys. Express 2 (2009) 057001.
[11] M. Stieger, W. Richtering, J.S. Pedersen, P. Lindner, J. Chem. Phys. 120 (2004) 6197.
[12] T.G. Mason, M.Y. Lin, Phys. Rev. E 71 (2005) 040801(R).
[13] J. Clara-Rahola, A. Fernandez-Nieves, B. Sierra-Martin, A.B. South, L.A. Lyon, J. Kohhlbrecher, A. Fernandez Barbero, J. Chem. Phys. 136 (2012) 214903.
[14] M. Reufer, P. Díaz-Leyva, I. Lynch, F. Scheffold, Eur. Phys. J. E 28 (2009) 165.
[15] S. Xu, J. Zhang, C. Paquet, Y. Lin, E. Kumacheva, Adv. Funct. Mater. 13 (2003) 468.
[16] J.M. Weissman, H.B. Sunkara, A.S. Tse, S.A. Asher, Science 274 (1996) 959.
[17] J.M. Cathcart, L.A. Lyon, M. Weck, R.D. Bock, Proc. SPIE 5403 (2004) 774.
[18] J. Liu, H.J. Schöpe, T. Palberg, Part. Part. Syst. Charact. 17 (2000) 206.
[19] W. Heller, Phys. Rev. 68 (1945) 5.
[20] M. Alexander, L.F. Rojas-Ochoa, M. Leser, P. Schurtenberger, J. Colloid Interface Sci. 24 (2002) 35.
[21] R. Hidalgo-Álvarez (Ed.), Structural and Functional Properties of Colloidal Systems, 146, CRC Press, Taylor and Francis Group, 2009, pp. 77–91.
[22] P. Schiebener, J. Straub, J.L. Sengers, J.S. Gallagher, J. Phys. Chem. Ref. Data 19 (1990) 677.
[23] A.P. Philipse, C. Smits, A. Vrij, J. Colloid Interface Sci. 129 (1989) 335.